The International Archives of the Photogrammetry, Remote Sensing and Spatial Information Sciences, Volume XLVIII-M-9-2025
30th CIPA Symposium "Heritage Conservation from Bits:
From Digital Documentation to Data-driven Heritage Conservation", 25–29 August 2025, Seoul, Republic of Korea

Challenges in 3D Integrated Surveying of Complex Historic Sites: The Case of Santa Maria della Steccata (Parma – Italy)

Andrea Zerbi [1], Nazarena Bruno [1], Sandra Mikolajewska [1], Riccardo Roncella [1]

[1] Dept. of Engineering and Architecture (DIA), University of Parma, Italy – (andrea.zerbi, nazarena.bruno, sandra.mikolajewska, riccardo.roncella)@unipr.it

Keywords: Cultural Heritage, 3D Survey, Data Co-registration, Spherical Photogrammetry, Laser-scanning, Accuracy Assessment.

Abstract

This article addresses the challenges of conducting integrated 3D surveys of complex historic architecture, focusing on the documentation and modelling of the Basilica of Santa Maria della Steccata in Parma (Italy). The Basilica's impressive scale, rich decorative features, and complex architectural layout – including a network of secondary spaces and attics accessible only through narrow, meandering paths – posed significant challenges for the survey. To overcome these obstacles, an integrated approach combining Terrestrial Laser Scanning (TLS), Close-Range Photogrammetry (CRP), Spherical Photogrammetry (SP), and UAV Photogrammetry was employed. The article outlines the planning, execution, and processing phases of the survey campaign, with particular emphasis on the methodological issues involved in merging data from multiple sources in such a constrained and heterogeneous environment. In this context, the article introduces and evaluates an ICP-assisted Bundle Block Adjustment (ICP-BBA) strategy designed to improve CRP- and TLS-derived models, demonstrating its effectiveness in enhancing local consistency in areas prone to residual misalignments. In addition, the performance of SP is examined under varying spatial conditions, highlighting its potential both as a supplementary method for areas with restricted accessibility and as a stand-alone alternative in specific use cases.

1. Introduction

This work originates from a scientific agreement between the Department of Engineering and Architecture of the University of Parma (Italy) and the General Secretariat of the Ministry of Culture for Emilia-Romagna Region (Italy). The project aimed to document the geometric, architectural and material characteristics of the Basilica of Santa Maria della Steccata in Parma, providing the essential knowledge for drafting a restoration project funded within the Italian National Recovery and Resilience Plan (PNRR). Despite being a major example of Renaissance architecture in the region, the Basilica has undergone systematic surveying only twice: once at the beginning of the 20th century (1904), and, again, toward its end (1982). Though significant for their time, both lacked the advanced methodologies now available, which enable levels of precision unimaginable just a few decades ago. This article presents the recent survey and modeling of the Basilica, focusing on the main challenges of integrating different surveying techniques and proposing methods for data fusion and validation.

The Church of Santa Maria della Steccata, elevated to the status of minor basilica in 2008, was originally built to house an image of the Virgin and Child, known as the "Madonna della Steccata". This image, dating back to the 14th century, is believed to have been painted within a small oratory located in the heart of the city. By the 15th century, it had become an object of widespread devotion and was considered miraculous. To protect it, the oratory was enclosed by a wooden fence – or *steccato* in Italian – from which the image took its name. In the early 16th century, the city authorities undertook a project to widen the streets and beautify the urban landscape, paying little heed to the buildings that would need to be demolished in the process. As a result, a third of the original oratory was torn down. To prevent further damage, the Confraternity of the Madonna della Steccata, founded in 1493, initiated the construction of a new church just a short distance from the original site. The foundation stone was laid in 1521.

It is now widely accepted that the execution plan for the new building was provided by Bernardino Zaccagni, with the support of his son Gian Francesco. However, most scholars agree that the Parma-born architect likely lacked cultural tools necessary to conceive such an ambitious design. In particular, Bruno Adorni (Adorni, 1982), while rejecting Vasari's attribution of the project to Bramante, identifies Leonardo da Vinci – who died in 1519, just a few years before construction began – and his concept of the church-as-monument as the true source of inspiration. Indeed, numerous drawings by Leonardo, who was in Parma in 1514 and spent extended periods in Milan at the court of the Sforza, show striking similarities to the grand church in Parma, notably characterized by its Greek-cross plan inscribed within a nearly perfect square.

This is not the place to delve into the complex and often troubled history of the church's construction. It is sufficient to note that the Zaccagnis were removed from the project in 1525 and were likely replaced by Giovan Francesco D'Agrate. The dome, with its external loggia encircling the drum, was almost certainly designed by Antonio da Sangallo the Younger, who was in Parma in 1526. The new church, by then completed, was consecrated on 23 February 1539. It houses important frescoes by Michelangelo Anselmi (some based on designs by Giulio Romano), and, most notably, by Francesco Mazzola, known as Parmigianino.

In 1718, the sanctuary – already removed from the original congregation that had built it – was donated by Francesco Farnese to the Constantinian Order of Saint George. Throughout the century, the building was completed with several late Baroque additions. Among these are notable features such as the large Knights' Choir, constructed by Edelberto dalla Nave behind the eastern niche between 1725 and 1730; the current Madonna altar and other altars located in the southern and northern niches; the balustrades, statues, and more generally, the entire decorative scheme now present around the roofs, which were altered for this purpose.

Figure 1. The Basilica of Santa Maria della Steccata in Parma. Top: aerial view of the exterior; Bottom: a view of the dome.

2. Challenges and Objectives of the Survey

The architectural survey of a historic monumental building such as the Basilica della Steccata – characterised by its considerable scale, intricate decorative details, complex spatial configuration, and a tightly constrained urban context – inevitably presents substantial challenges that can only be addressed through meticulous survey planning (Gao et al., 2020; Zachos and Anagnostopoulos, 2024).

As previously mentioned, the building is laid out on a Greek-cross plan with arms extending along the cardinal axes. Three of the arms, covered by barrel vaults, terminate in large semicircular apses topped by spherical domes. The fourth arm, to the east, culminates in the apse that houses the grand scenographic high altar from the 18th century, behind which the Choir of the Knights of the Constantinian Order can be glimpsed.

At the corners of the cross are four square-based towers, originally intended to serve a purely structural function and therefore not designed to be accessible. After the removal of the Zaccagnis, it was decided to open these lower-level towers and convert them into chapels for worship, each with an octagonal interior layout. Excluding the semicircular apses, the Greek cross and the four corner towers are inscribed within an almost perfect square with sides measuring approximately 31 meters. At the intersection of the two arms, above the drum, rises the large dome designed by Sangallo, whose springing level is situated about 31 meters above the floor. The building is further extended by secondary spaces located behind the Knights' Choir, and by a complex network of attic spaces and roof terraces.

Particularly intricate is the system of vertical paths connecting the ground floor to the upper levels. Four narrow spiral staircases (ca. 60 cm wide) are located within the four corner towers. Today, only the one accessible from the south-east chapel is usable. This staircase connects the ground floor to a room situated approximately 13 meters above, which opens onto the church interior through a small window in the southern arm. From this room, a straight, very narrow staircase leads up to the attic above the southeast tower. A further series of tight and irregular stairways allow access to the attic space surrounding the dome's drum. Finally, a small wooden ladder leads to the uppermost terrace above the roof structure.

These intricate volumes, combined with difficult accessibility, made data acquisition and co-registration challenging, while high detail was anyway needed for documenting decorations. The Basilica's location in the historic centre of Parma presented additional technical and logistical challenges. Rising to a height of approximately 45 metres, the church stands free on three sides, facing a square and adjacent streets, while the fourth side is attached to neighbouring buildings. The constant flow of pedestrians and vehicles made it impossible to restrict traffic, further complicating data acquisition. In addition, overhead trolleybus cables interfered with the surveying process, GPS reception was hindered by the surrounding buildings, and the dense network of local Wi-Fi signals disrupted the connectivity of certain instruments. To meet all these challenges, an integration of different instruments and methodologies was used, including Terrestrial Laser Scanning (TLS), Close-Range Photogrammetry (CRP), Spherical Photogrammetry (SP) and Unmanned Aerial Vehicle (UAV) photogrammetry, all supported by a georeferenced topographic control network.

3. Materials and Methods

3.1 Ground Control Topographic Network

A topographic control network, intended to serve as a reference framework for all the other surveying operations was first setup. As previously discussed, the configuration of the vertical circulation system – comprising spiral staircases and other spatially constrained transitional elements – made it impossible connecting the lower and upper sections of the building with a single unified network through its interior.

To address these challenge, 42 targets (Figure 2) were placed both inside and outside the building, easily identifiable in both laser scans and photographs: 10 on the lower exterior part of the sanctuary, 15 inside the church and adjacent service rooms, 3 in the room above the South-East chapel, and 14 at the terrace level.

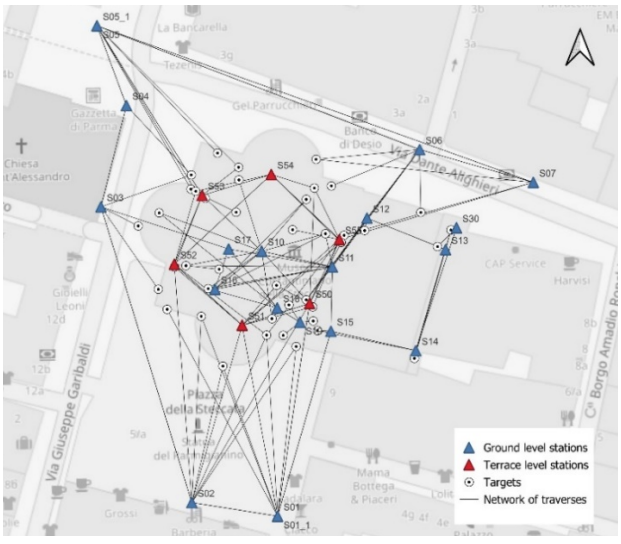

Figure 2. Topographic network of Ground Control Points.

Once positioned, the targets’ locations were determined through a topographic survey consisting of two closed and interconnected traverses. The first closed traverse, comprising 17 station points, was carried out at ground level and covered both the interior and exterior of the building, including the room previously mentioned; the second, made up of 6 station points, was conducted at the terrace level. The two closed traverses were connected using three mutually visible pairs of station points.

3.2 Terrestrial Laser Scanning

The TLS survey was conducted in all accessible internal and external areas using a Leica RTC 360 scan station. This device employs high-dynamic time-of-flight measurement, combined with Waveform Digitising (WFD), and is capable of recording up to 2,000,000 points per second over a range of 0.5 to 130 meters, with a spatial resolution of 3 mm at 10 meters. It is equipped with a Visual Inertial System (VIS), which integrates video data with an inertial measurement unit to track the scanner's position between setups.

During the TLS survey, the same challenges previously described were encountered, due to the impossibility of performing a single comprehensive scan set for the entire building due to difficulties with vertical connections. For this reason, a first set of scans was conducted for the lower part of the sanctuary, both inside and outside. To achieve exhaustive documentation of the building, capable of capturing both the architectural structure and decorative elements, 145 scans were acquired (Figure 3), generating a dataset exceeding eleven billion points. Subsequently, a second set of scans was carried out to document the upper exterior of the church and all the attic spaces. Thanks to better accessibility provided by the predominantly straight staircases, it was possible to include in this single set the scans of the South-East tower, extending up to the room located above the corresponding chapel. This second set consisted of 64 scans, totaling over two billion points.

During processing, the two laser scanner datasets were co-registered using an approach that combined cloud-to-cloud alignment with constraints from the topographic network. The black-and-white targets, placed on the external façades, inside the church, and on the rooftop terraces and previously surveyed via total station, were automatically detected in the point clouds and fixed to the coordinates estimated during the network adjustment. This integration resulted in a registration residual of 5 mm. At the end of the registration process, a unified dataset was obtained, comprising 209 scans and over thirteen billion points.

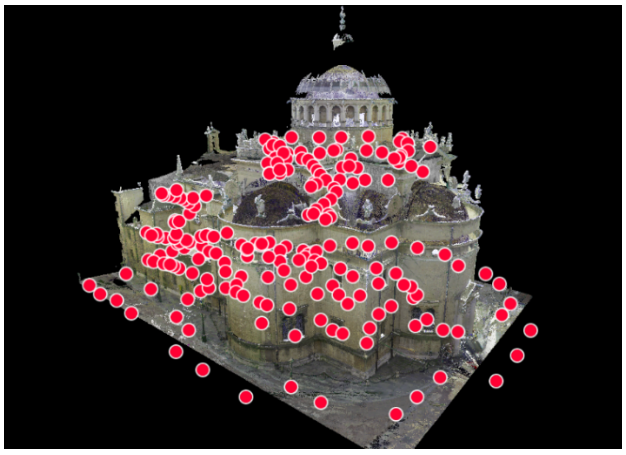

Figure 3. Point cloud obtained from TLS survey, with highlighted scan positions.

3.3 UAV and Close-Range Photogrammetry

To complement laser scanning and address areas not directly visible from ground level or terraces, photogrammetric methods were employed for the exterior of the building. These surveys enhanced spatial resolution at higher elevations and provided high-resolution orthophotos crucial for restoration planning. A total of 1065 images were acquired for this survey, with acquisition parameters summarized in Table 1. UAV photogrammetry was used to document all exterior façades and roofing systems, while areas accessible from the ground were also surveyed using a DSLR camera.

A DJI Mavic Mini drone was selected for UAV image acquisition: with a weight of less than 250 g, this UAV is classified as low-risk and is allowed to operate in restricted urban zones. The choice of this lightweight drone entailed a trade-off between regulatory compliance and technical capabilities: for instance, it lacks proximity sensors and does not support RTK modules for GNSS-assisted survey. Furthermore, the camera's resolution is suboptimal for metric applications.

	UAV1	UAV2	CRP1	CRP2
Equipment	DJI Mavic mini		Nikon d3x	
Resolution [pix]	4032x3024		6048x4032	
Camera asset	Nadir	Oblique	Nadir + Oblique	
Focal [mm]	24	24	35	18
Altitude/ distance to object [m]	55	14.5	13	13
GSD [mm/pix]	13.3	5.2	2.2	4.2
# img.	249	542	232	42

Table 1. Summary of the photogrammetric acquisitions.

Data acquisition was carried out in two separate steps: a nadir flight at an altitude of approximately 55 m to capture the site overview and roof structures (UAV 1 in Table 1), followed by a series of oblique flights with multi-altitude strips parallel to the vertical façades (UAV 2 in Table 1). Human-operated flight was chosen to maintain a higher level of responsiveness, particularly due to the presence of pigeons, which poses a risk to autonomous flight. As shown in Figure 4, this strategy enabled comprehensive coverage of the building, especially the upper sections of the façades, such as the cornices, which required high detail for restoration purposes.

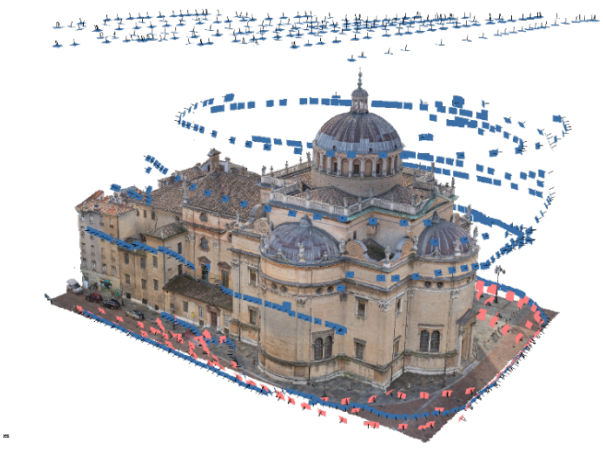

Figure 4. UAV and CR photogrammetric block. UAV imagery is represented in blue, CRP imagery in red.

From an operational standpoint, the urban context posed significant constraints for façade data acquisition: narrow streets prevented nadir image capture, while overhead tram cables limited UAV flight height for safety reasons. As a result, oblique images were acquired up to cornice level, and a low-altitude strip was manually collected with the UAV handheld. To enhance resolution and completeness on the façades, close-range photogrammetry with a Nikon D3x DSLR and wide-angle lenses (18–35 mm – CRP1 and CRP2 in Table 1) was integrated up to the first cornice level.

All 1065 acquired images were processed together using a standard Structure from Motion (SfM) workflow in Agisoft Metashape. Without RTK positioning, georeferencing relied solely on 22 Ground Control Points (GCPs) surveyed via total station. The use of natural features as additional GCPs was deliberately avoided, since architectural surfaces often presented worn or eroded edges, making the identification and collimation of natural points less reliable. Camera calibration was carried out on-the-job during Bundle Block Adjustment (BBA), taking into account the three different optical systems used.

3.4 Spherical Photogrammetry

To complement the TLS survey in particularly inaccessible or geometrically constrained areas of the Basilica's interior, spherical photogrammetry was employed. With its 360° field of view, SP is becoming an increasingly valuable tool for supplementing traditional survey techniques (Fangi, 2009; Koeva et al., 2017; Losè et al., 2021; Mandelli et al., 2017; Perfetti et al., 2024a).

Image acquisition specifically targeted the narrow vertical connections linking the ground level to the attic spaces, including the spiral staircase and the series of tight, irregular passages, to integrate and complete the overall spatial dataset. However, the survey was also deliberately extended to adjacent, more accessible areas – such as the corridor behind the choir, the south-east chapel, and the room at the top of the staircase (Room 1) – which had already been acquired through TLS. This overlap was designed to allow for a direct comparison between the two methods and to assess the accuracy and reliability of SP as both a supplementary and potentially alternative documentation technique in similarly constrained contexts. Figure 5 shows the complete path acquired from the choir to the attic.

The survey was conducted using the INSTA360 Pro2 spherical camera. This device features six equidistant sensors arranged around the equator of a 143 mm diameter spherical body. Each sensor captures 4000×3000 pixel images with a 200° field of view through fisheye lenses (focal length: 1.88 mm, aperture: F2.4). The camera records raw fisheye images and can optionally produce real-time stitched equirectangular panoramas (7680 × 3840 pixels).

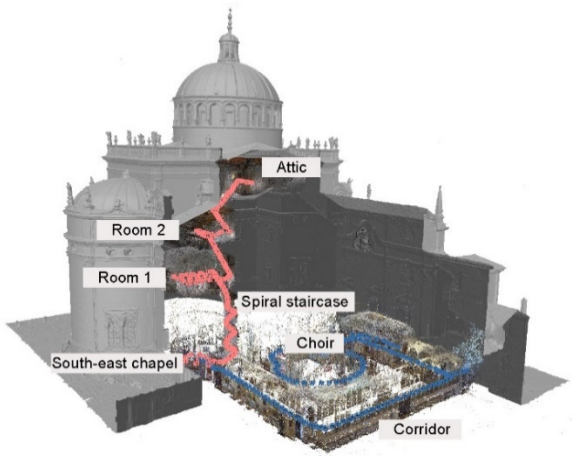

Figure 5. Spherical photogrammetric block inside the Basilica. SP1 dataset is represented in red, SP2 in blue.

The survey was carried out over two days: the first (SP1) covered the ascent path, and the second (SP2) the corridor behind the choir. In both cases, the camera was tripod-mounted and operated in single-shot mode to avoid capturing the operator and reduce motion blur in the low-light conditions characteristic of these spaces. As the access routes were largely unlit, three adjustable lights were mounted on the tripod and calibrated to balance illumination while avoiding overexposure, particularly due to the proximity of staircase walls. The average base-length between consecutive images was approximately 30 cm along staircases (one shoot per step) and about 1 m in larger rooms and corridors. To prioritize image quality, the ISO sensitivity was fixed at 100, limiting sensor noise. Table 2 provides a summary of the number of captured images, along with details on the shooting locations and acquisition durations. Also, for spherical imagery, the processing workflow was implemented using Agisoft Metashape.

Dataset	# img.	# Shooting points	Avg. GSD [mm/pix]	Time
SP1	1014	169	0.45	2 h
SP2	840	140	1.3	1 h

Table 2. Summary of the acquired data using INSTA 360.

Due to the physical arrangement of the camera's six sensors – non-coincident centres of projection with measurable offsets – assuming a single projection centre for stitched panoramic images would lead to significant geometric distortions. This is particularly critical in very confined spaces, where the parallax effects induced by sensor separation become more pronounced. For this reason, the processing was carried out directly on the individual raw fisheye images acquired by each sensor, rather than using the stitched equirectangular outputs, following the same methodology proposed in (Perfetti et al., 2024b).

To account for the fixed spatial relationships among the sensors, the image sets acquired from each shooting position were treated as part of a multi-camera system. A rigid constraint was imposed, defining the relative position and orientation of each sensor with respect to a designated master sensor. In this configuration, only the Exterior Orientation (EO) of the master camera is estimated during the BBA, while the orientations of the remaining sensors (slaves) are derived from fixed Relative Orientation (RO) parameters, assumed to be invariant across all acquisition positions. This strategy improves internal consistency and reduces the degrees of freedom in the adjustment process, which is particularly useful under limited control conditions. The SfM phase was initialized using nominal focal lengths provided by the manufacturer. All other Interior Orientation (IO) parameters, along with the RO between sensors, were refined during the BBA. The calibration model was an equidistant fisheye projection combined with the Brown distortion model.

Six black-and-white targets were employed as GCPs. Specifically, three of these were placed along the corridor behind the choir, and the remaining three within the intermediate room (Room 1). The rest of the photogrammetric block remained unconstrained. While this limited and localized distribution of GCPs is suboptimal from a strong geometric control perspective, previous studies (Bruno et al., 2024.; Perfetti et al., 2024b) have

demonstrated that the use of a multi-camera constraint can sufficiently ensure the stability of the photogrammetric solution.

3.5 Integrated Data Processing for Enhanced Co-registration

A first comparison between the two Digital Surface Models (DSMs), one obtained through integrated photogrammetric survey and the other via LiDAR scanning, shows that, overall, the co-registration of the two datasets is more than satisfactory, with average differences of less than 1 cm. Significantly larger discrepancies are found only in correspondence with the decorative elements of the façade (cornices, pediments, etc.), where the acquisition geometry can significantly affect the behaviour of the two instruments. The availability of a good network of control points to which both 3D reconstructions are referenced ensures proper co-registration of the data, making the use of alignment algorithms between the two models (such as Iterative Closest Points - ICP) almost unnecessary. However, as shown in Figure 6A, there are fairly large areas where differences slightly exceed 1 cm. While these are not excessive given the tolerances required for 1:50 scale drawings, they do indicate a systematic difference in how the two techniques represent those areas. This may result in greater difficulty for the human operator or a noisier output from automatic 3D reconstruction methods when combining the two datasets for the final reconstruction.

To improve model merging, a data fusion BBA routine, introduced in (Guccione et al., 2024) and inspired by pioneering works such as (Ebner and Strunz, 1988) and (Rosenholm and Torlegard, 1988) was employed in the experiment to evaluate its potential in enhancing data co-registration. The method is based on an innovative implementation of a 3D model-constrained aerial triangulation strategy. Within each iteration of the image bundle block adjustment, the nearest point on a reference surface is identified for every tie point using a KD-tree nearest neighbour search. A pseudo-observation (formulated analogously to GCP constraints) is then incorporated into the adjustment system. This observation acts to steer the photogrammetric solution towards the reference model, with influence modulated by a dedicated weighting strategy of the additional pseudo-observation. To mitigate the impact of outliers, these constraints are introduced only when the distance between the tie point and the reference surface falls below a specified threshold. In other words, the method can be regarded as an ICP-assisted Bundle Block Adjustment and will hereafter be referred to as such (ICP-BBA). Furthermore, as the ICP-BBA process iterates, the weights of the pseudo-observations are progressively increased, strengthening their influence on the final solution. The implementation leverages the capabilities of the *Ceres Solver* optimization library (Agarwal and Mierle, 2023), enabling efficient and robust solution of the underlying non-linear least squares problem.

From a methodological point of view, the proposed approach presents certain limitations, as it does not fully account for the stochastic characteristics of the different data sources involved. The reference 3D model (which potentially can be obtained from other instruments or surveys, not necessarily a laser scanner) is treated as immutable, with only the photogrammetric block being influenced during the ICP-assisted BBA. Achieving a true data fusion that incorporates the statistical properties of both datasets (photogrammetric and laser scanner) would require integrating the progressive co-registration of the laser scans themselves throughout the BBA iterations. However, this would introduce significant challenges in conditioning the adjustment system, given that the number of tie points is typically much smaller than the number of points constituting the scans, and it would demand substantial computational resources, likely disproportionate to the scale of the problem being addressed. A more methodologically sustainable solution is arguably the one adopted by certain software platforms (e.g., Agisoft Metashape from version 1.7 onward), in which laser scans are represented as equirectangular projections and treated as image-like entities (either in colour, when available, or grayscale based on TLS intensity values). These are oriented jointly with the actual photogrammetric images using a standard BBA process. This strategy, however, does not explicitly take into account the three-dimensional nature of the laser data, as the TLS range information is not used. In any case, as previously mentioned, the objective of this experiment was not to achieve a methodologically rigorous data fusion, but rather to align the photogrammetric and laser scanner datasets as closely as possible, to facilitate the final 3D model reconstruction.

4. Accuracy Assessment

4.1 TLS and CRP+UAV Comparison

The results obtained through the application of the ICP-BBA procedure described above are presented below. To better highlight the contribution of the method in more challenging scenarios, nadir images capturing the roof surfaces of the building were removed from the photogrammetric block in certain tests. These images typically increase the block's rigidity, thereby reducing potential drift effects in the photogrammetric solution (effects that are more likely to occur, for example, in terrestrial-only acquisition configurations).

Table 3 and Figure 6 present the outcomes obtained under the following conditions:

A. Using the traditional workflow/BBA, with the block referenced to topographic GCPs, all images included (nadir images as well), and the subsequent alignment of the photogrammetric and laser scanner models via ICP (Figure 6.A);
B. Using the traditional workflow/BBA but excluding nadir images and omitting the final ICP alignment step (Figure 6.B);
C. Applying the ICP-BBA procedure with a moderate weighting of the pseudo-observation equations, thereby enforcing a looser local adherence to the reference model and favouring the internal consistency of the photogrammetric block (Figure 6.C);
D. Applying the ICP-BBA procedure with higher weights assigned to the pseudo-observations, at the expense of the collinearity equation residuals (Figure 6.D).

	Min [mm]	Max [mm]	Average [mm]	Std. Dev. [mm]
A	-18.1	18.1	0.8	4.9
B	-18.1	18.1	0.0	5.7
C	-18.2	18.2	0.7	4.6
D	-18.1	18.1	0.6	4.5

Table 3. DSM comparison between TLS and photogrammetry in the exterior facades.

The values reported in Table 3 indicate relatively minor differences among the four configurations considered. Minimum and maximum distance values are essentially identical across all cases, as are the average values (notably, and somewhat unexpectedly, equal to zero in configuration B where no ICP was applied, although the mean values in the other cases remain

similarly low). Standard deviation values range from a minimum of 4.5 mm in case D (ICP-BBA with higher pseudo-observation weights), almost identical to case C (4.6 mm) to a maximum of 5.7 mm (approximately 27% higher) in case B, where a traditional BBA was performed using only topographic GCPs, without nadir imagery of the roof surfaces and without any ICP refinement.

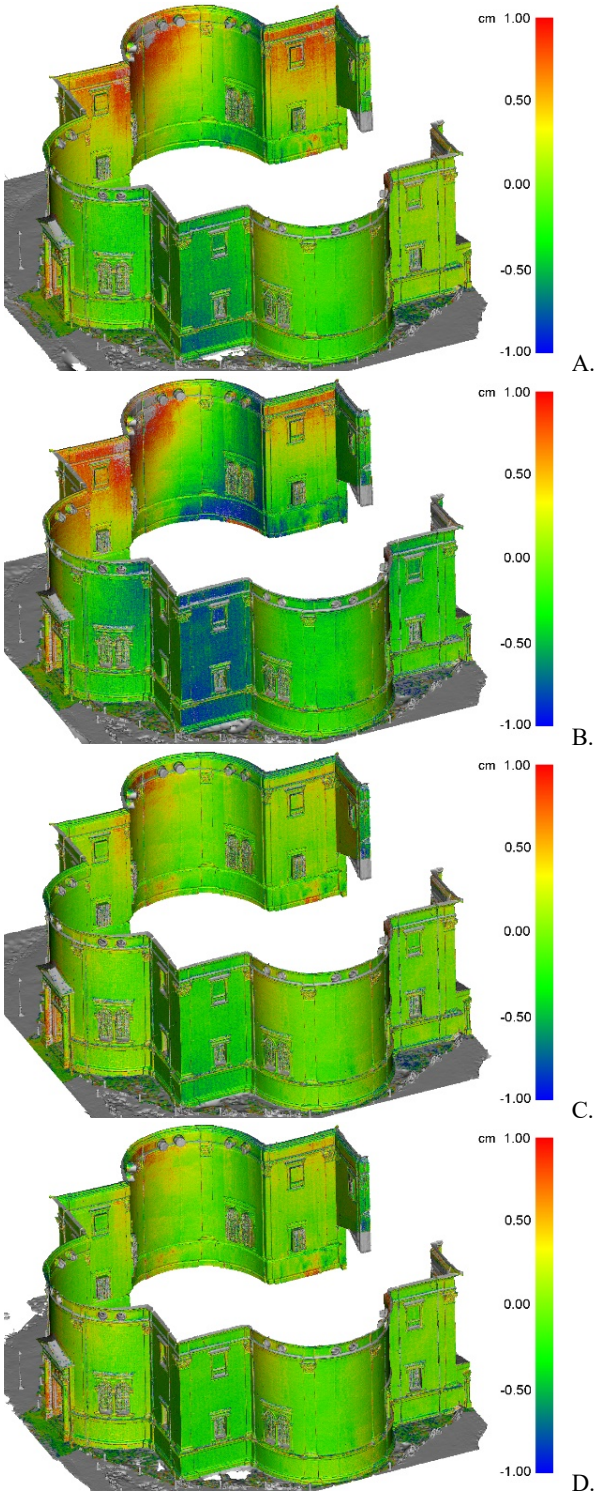

Figure 6. False-colour distance maps comparing DSMs from TLS and photogrammetry on the external façades. From top to bottom, the results correspond to different photogrammetric block processing configurations. The colour scale represents distance values ranging from -1 cm (blue) to +1 cm (red).

As far as the different weighting strategy adopted in ICP-BBA is concerned, even if the stronger constraint given by the configuration D provides better distances-to-reference statistics, it also increases significantly the collinearity residuals of the image points (0.65 pixel in case C vs. 1.06 pixel in case D). Determining whether the increased residuals had a tangible impact on the reconstruction is not straightforward; however, it can be hypothesized that poorer intersection geometry between corresponding projection rays may result in reduced matching accuracy. Consequently, solution C is probably preferrable.

A closer inspection of Figure 6 and Figure 7, the latter showing the histograms of the distances between the photogrammetric and reference (LS) models, clearly illustrates the improvement introduced by the ICP-BBA approach. In many areas where the initial alignment between the two models was already very good, the solution remains unchanged. Conversely, in portions of the model where more significant localized differences are observed (still within a range of approximately 10 mm), likely due to minor drift effects in the photogrammetric solution rather than misregistration of the LS scans, the application of ICP-BBA results in an improved reconstruction. In these cases, the distance histograms appear much more symmetric around the mean value and show a significantly lower frequency of discrepancies in the 2–8 mm range.

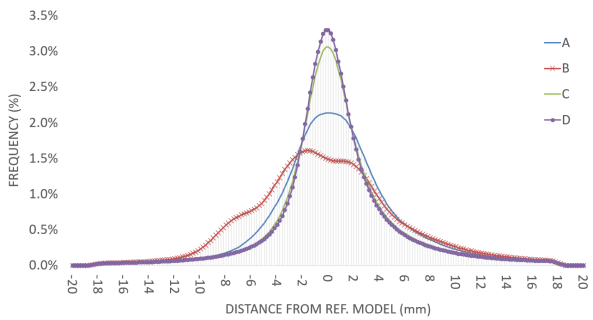

Figure 7. Distribution of distances values of the photogrammetric 3D model from the reference one (TLS).

4.2 TLS and Spherical Photogrammetry (SP) Comparison

To assess the orientation accuracy of the spherical photogrammetry block, 50 Check Points (CPs) were identified and compared against the corresponding coordinates extracted from the TLS dataset (considered again as the reference), within the areas where the two acquisitions overlapped.

As described in Section 3.4, two separate acquisitions were carried out (SP1 and SP2), conducted on different days and covering areas with distinct geometric characteristics. While the goal was to process the two datasets together as a single block, two alternative approaches to camera calibration were tested to determine the most effective strategy for IO parameter estimation and the effect of different estimations on the results. In the first approach, a single shared calibration set (Calib.1) was estimated during the BBA and applied across both datasets. In the second, independent calibration parameters (Calib.2a and Calib.2b) were estimated separately for each dataset, taking into account the different acquisition conditions and environments.

Table 4 summarizes the results, in terms of reprojection error, Root Mean Square Error (RMSE) on GCPs and CPs as well as the minimum, maximum, and mean CP residuals, in order to highlight the variability range within the dataset. The findings demonstrate that the choice between single and dual calibration

has a significant impact on orientation accuracy. When a single calibration set was applied across both datasets, the RMSE on the CPs reached 48.5 mm, with a maximum deviation of 74.9 mm. In contrast, using two separate calibration sets significantly improved accuracy, reducing the RMSE to 24.2 mm and the maximum error to 46.5 mm. A similar trend is observed for the GCPs: while the dual-calibration approach yielded an RMSE of just under 10 mm, the single-calibration setup resulted in residuals around 40 mm.

Calib. sets	Reproj. error [pix]	GCPs RMSE [mm]	CPs			
			Min. [mm]	Max. [mm]	Mean [mm]	RMSE [mm]
Calib1	0.97	40.4	2.7	74.9	43.3	48.5
Calib 2a Calib 2b	0.95	9.9	3.7	46.5	21.7	24.2

Table 4. Residuals on GCPs and CPs of the spherical photogrammetry dataset compared to TLS data.

This performance gap appears to be influenced not only by the different acquisition days but also by the distinct spatial characteristics of the surveyed areas. Specifically, the SP1 dataset includes the most confined areas – such as stairwells and narrow passages – while SP2 covers more open spaces, including the corridor and part of the Basilica's choir. The difference in average scene depth likely affected the calibration process, particularly the estimation of the focal length.

A more detailed analysis of the calibration results confirms that the most significant variation between the configurations lies in the focal length parameter. Figure 8 shows the estimated focal length values for each sensor across the different calibration sets. Notably, the focal length derived from the single-calibration set (Calib.1) tends to fall between the values estimated from the two separate calibrations (Calib.2a and Calib.2b). Although these differences are small in absolute terms – on the order of 2/1000 pixels – they turned in substantial discrepancies in the residuals on both GCPs and CPs.

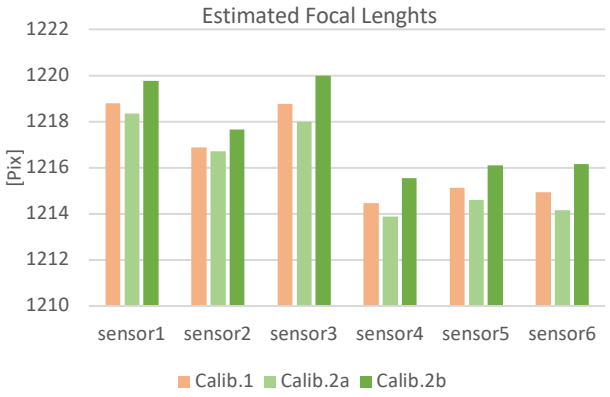

Figure 8. Estimated focal length values for each sensor across the different calibration sets. Parameters from the Calib.1 set are shown in orange, while those from Calib.2a and Calib.2b are represented in two different shades of green.

The analysis of CPs residual variability and spatial distribution reveals a correlation with both the GCP distribution and the size of the surveyed areas – hence with the camera-to-object distance. Figure 9 shows the location of GCPs and CPs, along with their associated error ellipses, while Figure 10 presents the median residual values and the variability range (from minimum to maximum) of the CPs, grouped by spatial zones within the Basilica (ordered by increasing spatial extent: Room 2, Attics, Corridor, South-East Chapel and Choir).

As expected, the highest median residuals are observed in the choir, where values range from 23 mm to a maximum of 43 mm. This area is the farthest from any GCPs and with the highest GSD (Ground Sampling Distance). Interestingly, the same pattern does not occur at the opposite end of the survey path, in the attic, despite its being accessible only through a long and complex route involving narrow staircases. In the attic, residuals remain below 27 mm, with a median value around 20 mm. This suggests that, beyond GCP distribution, the spatial characteristics of each area – particularly its size and geometry – also influence the accuracy of the photogrammetric solution.

For example, the south-east chapel, although located relatively close to a GCP, shows high residuals, with a maximum of 46.5 mm. This value corresponds to a check point on the dome of the chapel, about 8 meters above the average image acquisition height (red ellipse in Figure 9). Similarly, in the choir, the large scale of the space places all CPs at a significant distance from the camera positions, leading to worse image scale and, consequently,

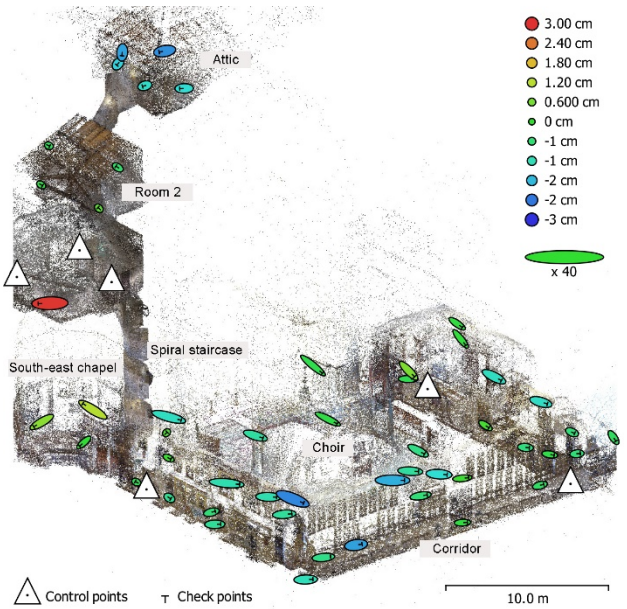

Figure 9. GCP and CP locations and residual estimates. Z residual is represented by ellipse colour. X,Y residuals are represented by ellipse shape.

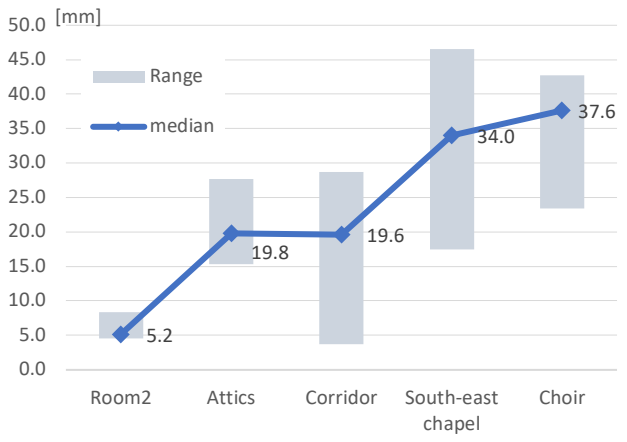

Figure 10. CPs RMSE variability grouped by spatial zones.

reduced geometric accuracy. In contrast, the corridor behind the choir is both relatively well constrained by GCPs and has a tunnel-like configuration, meaning that its surfaces remain consistently close to the image acquisition points. As a result, the RMSE in this area is comparatively low, with the highest residuals found on CPs located on the vaulted ceiling.

5. Conclusion

This article addressed the challenges of conducting integrated 3D surveys of complex historic architecture, focusing on the documentation and modelling of the Basilica of Santa Maria della Steccata in Parma (Italy). The survey addressed significant challenges posed by the building's considerable scale, its richly decorated surfaces, and the intricate spatial articulation, including a network of secondary and attic spaces accessible only via narrow, winding staircases. To achieve a complete and detailed representation, an integrated survey strategy was adopted, combining Terrestrial Laser Scanning, Close-Range, Spherical, and UAV Photogrammetry. Beyond achieving spatial completeness, the central aim was to understand how to effectively merge heterogeneous datasets, maximizing geometric accuracy while minimizing residual inconsistencies.

In this context, the article introduced and evaluated a hybrid registration method – ICP-assisted Bundle Block Adjustment (ICP-BBA) – which combines point cloud alignment with photogrammetric BBA. The approach proved effective in improving local coherence across datasets, particularly in areas where residual misalignments are most pronounced.

The performance of spherical photogrammetry was also critically assessed across different spatial conditions. SP proved to be a highly valuable solution for capturing areas that are either inaccessible or unsuitable for traditional survey instruments. Its effectiveness was especially notable in confined environments, where short and relatively constant distances between camera and object preserve geometric consistency. However, in larger spaces, performance worsened as increasing distances led to reduced image resolution and greater positional uncertainty. While the 360° field of view allows for efficient coverage, the findings suggest that acquisition strategies must be adapted to the geometry of the space, by increasing the number of images, introducing additional strips, even at different height from the ground.

In conclusion, the experience at the Basilica della Steccata confirms the necessity and viability of multi-sensor approaches in complex architectural contexts. However, true integration has yet to be fully achieved: one dataset typically acts as the geometric reference, while others are adjusted to fit, revealing an underlying hierarchical relationship. The effectiveness of the integration, however, hinges on thoughtful planning and calibration of both instruments and processing strategies.

Acknowledgements

The project was partially funded under the National Recovery and Resilience Plan (PNRR), Mission 4 Component 2 Investment 1.5–Call for tender No. 3277 of 30/12/2021 of the Italian Ministry of University and Research funded by the European Union–NextGenerationEU. Project code ECS00000033, Concession Decree No. 1052 of 23/06/2022 adopted by the Italian Ministry of University and Research, No. CUP D93C22000460001, "Ecosystem for Sustainable Transition in Emilia-Romagna" (Ecosister), Spoke 4.

References

Adorni, B., 1982. Santa Maria della Steccata a Parma. Artegrafica Silva, Parma.

Agarwal, S., Mierle, K., 2023. Ceres Solver — A Large Scale Non-linear Optimization Library.

Bruno, N., Perfetti, L., Fassi, F., & Roncella, R. (2024). Photogrammetric survey of narrow spaces in cultural heritage: Comparison of two multi-camera approaches. *International Archives of the Photogrammetry, Remote Sensing and Spatial Information Sciences*, *48*(2/W4-2024), 87-94.

Ebner, H., & Strunz, G. (1988). Combined point determination using digital terrain models as control information. *International Archives of Photogrammetry and Remote Sensing*, *27*(B11/3), 578-587.

Fangi, G. (2009, October). Further developments of the spherical photogrammetry for cultural heritage. In *XXII Cipa Symposium, Kyoto* (pp. 11-15).

Gao, X., Shen, S., Zhu, L., Shi, T., Wang, Z., Hu, Z., 2020. Complete scene reconstruction by merging images and laser scans. *IEEE Transactions on Circuits and Systems for Video Technology* 30, 3688–3701.

Guccione, D. E., Turvey, E., Roncella, R., Thoeni, K., & Giacomini, A. (2024). Proficient Calibration Methodologies for Fixed Photogrammetric Monitoring Systems. *Remote Sensing*, *16*(13), 2281.

Koeva, M., Luleva, M., Maldjanski, P., 2017. Integrating Spherical Panoramas and Maps for Visualization of Cultural Heritage Objects Using Virtual Reality Technology. *Sensors* 2017, Vol. 17, Page 829 17, 829.

Teppati Losè, L., Chiabrando, F., & Giulio Tonolo, F. (2021). Documentation of complex environments using 360 cameras. The Santa Marta Belltower in Montanaro. *Remote Sensing*, *13*(18), 3633.

Mandelli, A., Fassi, F., Perfetti, L., & Polari, C. (2017). Testing different survey techniques to model architectonic narrow spaces. *International archives of the photogrammetry, remote sensing and spatial information sciences*, *42*, 505-511.

Perfetti, L., Fassi, F., & Vassena, G. (2024a). Ant3D—A Fisheye Multi-Camera System to Survey Narrow Spaces. *Sensors*, *24*(13), 4177.

Perfetti, L., Bruno, N., & Roncella, R. (2024b). Multi-Camera Rig and Spherical Camera Assessment for Indoor Surveys in Complex Spaces. *Remote Sensing*, *16*(23), 4505.

Rosenholm, D. A. N., & TORLEGARD, K. (1988). Three-dimensional absolute orientation of stereo models using digital elevation models. *Photogrammetric engineering and remote sensing*, *54*(10), 1385-1389.

Zachos, A., & Anagnostopoulos, C. N. (2025). Using TLS, UAV, and MR methodologies for 3D modelling and historical recreation of religious heritage monuments. *ACM Journal on Computing and Cultural Heritage*, *17*(4), 1-23.